Journal of Asian Earth Sciences 40 (2011) 1151–1163

Contents lists available at ScienceDirect

Journal of Asian Earth Sciences

journal homepage: www.elsevier.com/locate/jseaes

Comparison of speleothem $\delta^{18}O$ records from eastern China with solar insolation, ice core and marine records: Similarities and discrepancies on different time scales

Naijung Wan [a], Weiling Chung [b], Hong-Chun Li [a,d,e,*], Huilin Lin [b], Teh-Lung Ku [c], Chuan-Chou Shen [d], Daoxian Yuan [e], Meiliang Zhang [f], Yushi Lin [f]

[a] Department of Earth Sciences, National Cheng-Kung University, Tainan 70101, Taiwan, ROC
[b] Institute of Marine Geology and Chemistry, National Sun Yat-sen University, Kaohsiung 804, Taiwan, ROC
[c] Department of Earth Sciences, University of Southern California, Los Angeles, CA 90089, USA
[d] High-precision Mass Spectrometry and Environment Change Laboratory (HISPEC), Department of Geosciences, National Taiwan University, Taipei 10617, Taiwan, ROC
[e] School of Geographical Sciences, Southwest University of China, Chongqing 400715, China
[f] The Key Karst Laboratory of Dynamics, Institute of Karst Geology, CAGS, Guilin, China

ARTICLE INFO

Article history:
Available online 30 June 2010

Keywords:
Oxygen isotopes
Stalagmite
Summer monsoon
Solar insolation
Regional climate
Global climate

ABSTRACT

Four ^{230}Th-dated $\delta^{18}O$ records in three stalagmites: one from Dragon Spring (stalagmite L12) and two from Golden Lion Caves (stalagmites JSD-01 and JSD-02) located in Libo County, southeast Guizhou, China, are presented. These records cover age ranges of 0.75–2 ka (late Holocene), 9–9.6 ka (early Holocene), 87.9–88.2 ka and 93.8–95.2 ka (late Pleistocene). They fit well with the published Dongge Cave record from the same area, where the climate has been much influenced by the East Asian Monsoon. The agreement reinforces the role of stalagmite $\delta^{18}O$ as a proxy for regional precipitation or monsoon strength. On millennial or longer time scales, the $\delta^{18}O$ record of Dongge Cave resembles those of Sanbao Cave in Hubei and Hulu Cave in Jiangsu of China. The matching of these records with the northern hemisphere solar-insolation variations points to the importance of insolation in affecting the East Asian Summer Monsoon strength on 10^3–10^4-yr scales. While the monsoon variations as depicted by these Chinese speleothem $\delta^{18}O$ records show a strong coupling to insolation's precession component (23-kyr period), other climate records of global significance extracted from oceanic and terrestrial deposits (e.g., deep-sea sediments, polar ice cores, cave deposits from non-monsoonal regions) do not. Although the latter records were thought to be also influenced by the large changes in global ice volume, they show variations modulated chiefly by insolation due to earth's eccentricity change (100-kyr period). It is hypothesized that precession variations control the distribution of solar insolation between the northern and southern hemispheres, the ITCZ position and the modulation of low-latitude summer monsoon variability. Increasing rainfall and/or summer/winter precipitation ratio brought about by strong summer monsoons leads to $\delta^{18}O$ depletion in stalagmites grown in monsoonal regions. One should use caution to compare speleothem $\delta^{18}O$ records with other paleoclimate records reflecting Pleistocene ice ages on 10^4–10^5-yr timescales.

1. Introduction

The East Asian Monsoon (EAM) plays an important role in affecting precipitation and temperature over the vast and densely populated region of eastern China. It is responsible for the generally cold/dry winter and warm/wet summer climates in the region. Knowledge on the linkage between the monsoonal system and global climate and on the system's sensitivity to changes in its forcing by orbital-controlled solar insolation and ocean circulation is not only of intrinsic scientific interest, but also of practical value in future climate predictability. Studies of past changes of EAM via Chinese loess records showed strong summer monsoon/weak winter monsoon during interglacial periods and weak summer monsoon/strong winter monsoon during glacial intervals (Ding et al., 1995; Liu et al., 1999; An, 2000). Earlier studies (e.g., Ding et al., 1995, 2002) have used the marine record of SPECMAP $\delta^{18}O$ to tune the chronology of continental records in China, based on this interglacial warm-wet vs. glacial cold-dry concept and assuming synchronous response to orbital forcing by both regional and global climates.

More recently, it has been shown that $\delta^{18}O$ of summer monsoon rains in China is negatively correlated with both rainfall amount and temperature, with rainfall amount being more influential to

* Corresponding author at: Department of Geosciences, National Taiwan University, Taipei 106, Taiwan, ROC. Tel.: +886 2 33662929; fax: +886 2 23636095.
E-mail address: hcli1960@ntu.edu.tw (H.-C. Li).

1367-9120/$ - see front matter © 2010 Elsevier Ltd. All rights reserved.
doi:10.1016/j.jseaes.2010.06.010

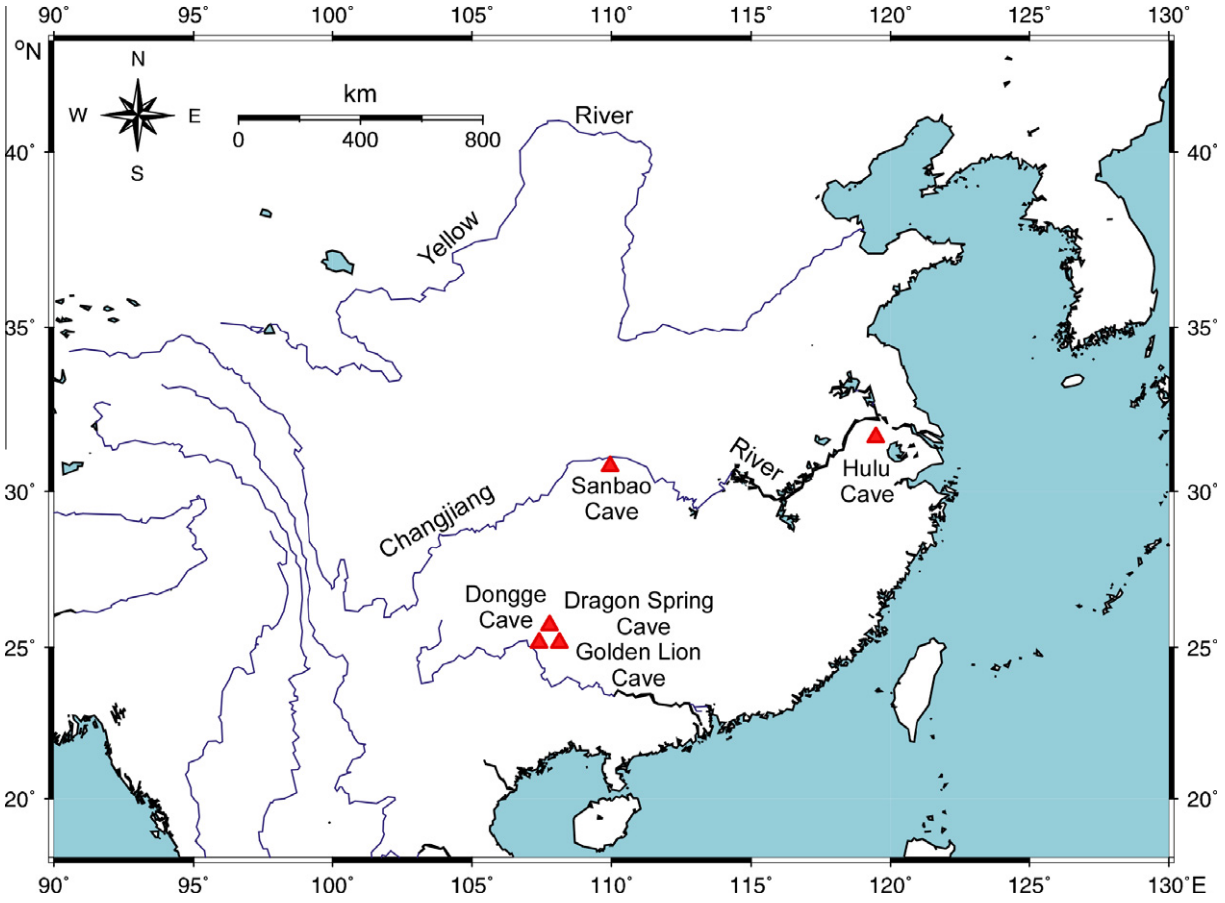

Fig. 1. Location map of the study area. Red tri-angles denote the locations of Dongge, Dragon Spring and Golden Lion Caves in Guizhou, Sanbao Cave in Hubei, and Hulu Cave in Nanjing.

the $\delta^{18}O$ signal (Johnson and Ingram, 2004; Li et al., 2007). A negative correlation between speleothem $\delta^{18}O$ and precipitation was also noted by Li et al. (1998). This has led to the increasing use of cave speleothem $\delta^{18}O$ to reconstruct paleo-monsoon variations (e.g., Li et al., 1998, 2005; Ku and Li, 1998; Paulsen et al., 2003; Wang et al., 2001, 2005, 2008; Yuan et al., 2004; Cosford et al. 2008; Hu et al., 2008). Such reconstructions showed strong correlations with changes in a number of phenomena including: northern hemisphere (NH) precession-modulated insolation, Greenland temperature, mid-high latitude sea surface temperature (SST), ocean and atmosphere circulation, and ITCZ position (Burns et al., 2003; Bar-Matthews et al., 2003; Fleitmann et al., 2003; Dykoski et al., 2005; Cruz et al., 2005; Asmerom et al., 2007; Shakun et al., 2007; Cosford et al., 2008; Wang et al., 2001, 2005, 2008). These correlations render speleothem $\delta^{18}O$ records as valuable archives for monsoon climates and as a tool for correlating and calibrating global climate records (Wang et al., 2008). The latter aspect of tool usage stems from the observation that tropical/subtropical monsoons respond mainly to changes in NH summer insolation on orbital timescales and their cyclic variations appear to be globally teleconnected in an exceptional fashion.

However, several studies have found that the Asian Summer Monsoon strength has time/phase lags with solar insolation and other global climatic records (e.g., Li et al., 2005; Kelly et al., 2006; Clemens et al., 1991; Clemens and Prell, 2007; Waelbroeck et al., 2008). Therefore, questions can be raised as to what extent the Asian Summer Monsoon links to other climatic systems on orbital scales, and how the precession-driven solar radiation changes affect the Asian Summer Monsoon, high-latitude climate, and global ice volume on orbital scales. In this study, we first present three stalagmite $\delta^{18}O$ records from Libo County of Guizhou, China. We then compare these records with the previously published $\delta^{18}O$ record of Dongge Cave from the same area. The Dongge Cave records, together with the records from Sanbao Cave (Hubei Province) and Hulu Cave (Jiangsu Province), are further compared with the NH solar insolation changes and with other climatic records of global significance. Through the comparisons, we seek to understand the cause for the correlations among the stalagmite $\delta^{18}O$ records from eastern China and their correlations to the precession-driven solar radiation, as well as the cause for the discrepancies between these time series and other global climatic records.

2. Background information of the study area

2.1. East Asian Monsoon (EAM)

The EAM and the Indian Monsoon (IDM) constitute the Asian Monsoon system (Wang, 2007). Having distinctive summer and winter wind regimes, the EAM forms as a result of thermal differences between the Asia landmass and the Pacific Ocean, and is thus affected by the altitude of Tibetan Plateau. Its circulation and associated precipitations are largely affected by the cold air mass from northern high latitudes, the warm water mass from the Equator, and interactions of air-sea circulations between the West Pacific Warm Pool and the Inter-tropical Convergence Zone (ITCZ) (Gao and Xu, 1962; Zhao and Wang, 1979; Tao and Chen, 1988; Chen et al., 1991; Zhang and Liu, 1992; Broecker, 1994a,b; Thompson

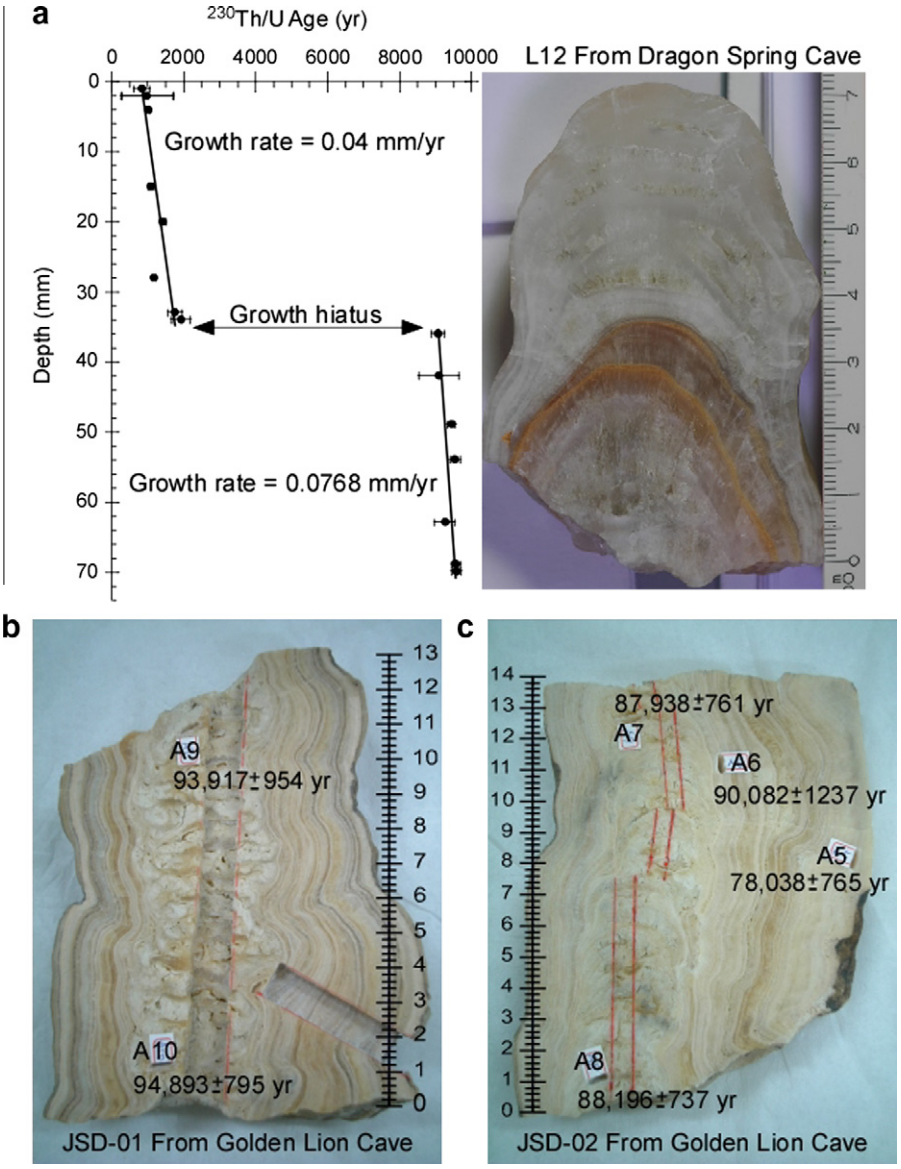

Fig. 2. Photos of the studied stalagmites. (a) Stalagmite L12. In the left panel, ^{230}Th dates, growth rates and age-depth relationship in L12 are shown. A growth hiatus exists at 35 mm depth. (b) and (c) Photos of stalagmites JSD-01 and JSD-02, respectively. ^{230}Th dates and sampling tracks for stable isotope analyses are shown.

et al., 1997; An, 2000). In the NH winter season, cold air from high latitudes controlled by the continental high-pressure system propagates southward along the eastern margin of the Tibetan Plateau to form the strongest northerly dry and cold winter monsoon in the world. This winter monsoon can extend to tropical South China and even cross the Equator to trigger southern hemisphere (SH) summer monsoons (An, 2000). During the summer, warm and humid air originating from low-latitude oceans can extend northwestward into China's interior as far as the China-Mongolia border, forming world's northernmost summer monsoon (An, 2000; Wang, 2007). The EAM climate is characterized by prominent seasonal changes in wind direction, precipitation and air temperature between cold/dry winter and hot/humid summer (An, 2000). In this study, we focus on the East Asian Summer Monsoon (EASM), an important precipitation source in eastern China. Paleomagnetic studies of Chinese loess deposits show significant EASM variations over the past 0.8 Myr, increasing during interglacial and decreasing during glacial periods (Liu et al., 1999). Precisely dated speleothem records with lighter δ^{18}O denoting stronger EASM have provided a history of EASM with high temporal resolutions (Wang et al., 2001; Yuan et al., 2004). Wang et al. (2008) reported changes in EASM over the past 220 kyr based on the speleothem δ^{18}O records from Dongge Cave in Guizhou, Sanbao Cave in Hubei and Hulu Cave in Jiangsu (Fig. 1). The changes correlated well with solar-insolation variations at 30–60°N: higher insolation correlated with stronger EASM. EASM changes on millennium or shorter time scales have also been studied using the speleothem δ^{18}O proxy, forming the viewpoint that lighter δ^{18}O results from heavier precipitation brought about by stronger EASM (Li et al., 1998; Paulsen et al., 2003; Wang et al., 2005). While the increase of NH solar insolation is thought to provide the forcing mechanism for enhanced EASM and precipitation in eastern China (Wang et al., 2001, 2005; Zhang et al., 2008), it remains uncertain whether such a forcing operates on sub-millennium scales as recorded by speleothem δ^{18}O (Zhang et al., 2010).

2.2. Golden Lion and Dragon Spring Caves

The two caves from which we studied the speleothem δ^{18}O records are located in Libo County in southeast Guizhou, in a transi-

Table 1
^{230}Th dating result of stalagmites L12, JSD-01 and JSD-02 from caves in Libo County, southeast Guizhou, China.

Sample number	Depth (mm)	^{238}U (ppb)	^{232}Th (ppt)	$\delta^{234}U_{measured}$[a]	$^{230}Th/^{238}U_{activity}$[c]	$^{230}Th/^{232}Th$ (ppm)[d]	Age uncorrected	Age corrected[c,e]	$\delta^{234}U_{initial}$ corrected
L12									
A1	1	89.8 ± 0.2	119.9±.9.12.7	133.3 ± 4.5	0.0099 ± 0.0023	122 ± 30.9	954 ± 221	868 ± 225	134 ± 5
V1	2	89.1 ± 0.4	1729.5 ± 18.3	129.2 ± 9.6	0.0231 ± 0.0034	20 ± 2.9	2260 ± 338	1002 ± 715	130 ± 10
V2	4	223.9 ± 0.8	273.8 ± 6.4	118.9 ± 3.8	0.0113 ± 0.0005	153 ± 8.1	1112 ± 54	1032 ± 67	119 ± 4
V3	15	223.9 ± 0.6	286.3 ± 6.3	119.4 ± 2.9	0.0122 ± 0.0006	158 ± 8.5	1197 ± 59	1114 ± 72	120 ± 3
V4	20	183.2 ± 0.9	81.4 ± 6.5	121.5 ± 5.9	0.0150 ± 0.0007	558 ± 52.2	1472 ± 72	14,423 ± 74	122 ± 6
V5	28	204.7 ± 0.6	239.3 ± 6.1	122.4 ± 3.3	0.0126 ± 0.0006	178 ± 9.7	1232 ± 60	1204 ± 62	123 ± 3
V6	33	303.0 ± 1.2	4619.2 ± 15.0	126.8 ± 3.5	0.0128 ± 0.0006	24 ± 0.7	2136 ± 61	1777 ± 189	127 ± 3
A2	34	248.7 ± 0.6	4910.9 ± 19.0	130.3 ± 3.2	0.0246 ± 0.0011	21 ± 1.0	2405 ± 113	1942 ± 258	131 ± 3
A3	36	273.2 ± 0.6	3190.4 ± 16.4	262.3 ± 2.4	0.1032 ± 0.0014	146 ± 2.1	9290 ± 132	9046 ± 180	269 ± 2
V7	38	298.9 ± 0.9	62486.9 ± 480.4	246.0 ± 3.4	0.2162 ± 0.0054	17 ± 0.4	20,677 ± 567	7842 ± 6867	251 ± 6
V8	42	333.7 ± 1.2	6275.5 ± 20.7	266.5 ± 3.6	0.1128 ± 0.0012	99 ± 1.1	10,153 ± 119	9073 ± 555	273 ± 4
V9	49	320.7 ± 1.1	466.6 ± 7.1	266.4 ± 4.2	0.1058 ± 0.0011	1200 ± 21.4	9496 ± 105	9412 ± 112	274 ± 4
V10	54	316.8 ± 1.2	302.0 ± 6.1	265.3 ± 4.5	0.1065 ± 0.0015	1844 ± 44.3	9573 ± 141	9519 ± 143	272 ± 5
V11	63	314.9 ± 1.1	414.4 ± 7.7	266.3 ± 4.2	0.1038 ± 0.0030	1302 ± 44.2	9309 ± 280	9233 ± 282	273 ± 4
V12	69	359.5 ± 1.0	783.5 ± 7.5	260.6 ± 3.4	0.1071 ± 0.0010	811 ± 10.3	9665 ± 94	9540 ± 112	268 ± 3
A4	70	266.3 ± 0.6	869.4 ± 12.8	263.9 ± 2.7	0.1070 ± 0.0014	541 ± 10.4	9628 ± 129	9560 ± 133	271 ± 3
JSD-02									
A5	Outer side	98.2 ± 0.2	342.9 ± 7	254.6 ± 4.2	0.6546 ± 0.0038	3094 ± 66.4	78,108 ± 762	78,038 ± 765	317 ± 5
A6	Inner side	626.2 ± 1.2	530.0 ± 9	417.7 ± 2.6	0.8245 ± 0.0075	16,084 ± 298.9	90,097 ± 1237	90,082 ± 1237	539 ± 4
A7	13	117.4 ± 0.2	560.6 ± 7	256.0 ± 3.1	0.7117 ± 0.0036	2461 ± 32.0	88,034 ± 756	87,938 ± 761	328 ± 4
A8	126	103.9 ± 0.2	299.5 ± 6.7	413.2 ± 4.0	0.8101 ± 0.0039	4639 ± 105.3	88,245 ± 736	88,196 ± 737	530 ± 5
JSD-01									
A9	16	134.6 ± 0.3	427.3 ± 7.0	348.1 ± 5.5	0.8029 ± 0.0040	4176 ± 70.8	93,975 ± 953	93,917 ± 954	454 ± 7
A10	121	115.8 ± 0.2	1672.3 ± 6.7	298.7 ± 3.2	0.7772 ± 0.0034	889 ± 5.1	95,168 ± 748	94,893 ± 795	391 ± 4

Analytical errors are 2σ of the mean.
Decay constants are 9.1577×10^{-6} yr^{-1} for ^{230}Th, 2.8263×10^{-6} yr^{-1} for ^{234}U, and 1.55125×10^{-10} yr^{-1} for ^{238}U(Cheng et al., 2000).
Those are the values for a material at secular equilibrium, with the crystal $^{232}Th/^{238}U$ value of 3.8. The errors are arbitrarily assumed to be 50%.
[a] $\delta^{234}U = ([^{234}U/^{238}U]_{activity} - 1) \times 1000$.
[b] $\delta^{234}U_{initial}$ corrected was calculated based on ^{230}Th age (T), i.e., $\delta^{234}U_{initial} = \delta^{234}U_{measured}Xe^{\lambda 234T}$, and T is corrected age.
[c] $^{230}Th/^{238}U_{activity} = 1 - e^{-\lambda 230T} + (\delta^{234}U_{measured}/1000)[\lambda_{230}/(\lambda_{230} - \lambda_{234})](1 - e^{-\lambda 230T - \lambda 234T})$, where T is the age.
[d] The degree of detrital ^{230}Th contamination is indicated by the $^{230}Th/^{232}Th$ atomic ratio instead of the activity ratio.
[e] Age corrections were calculated using an [$^{230}Th/^{232}Th$] atomic ratio of 4(±4) ppm.

tion area between the Yunnan-Guizhou Plateau and the Guangxi Basin. The mountainous Guizhou Province occupies an area of 176,100 km^2 in southwest China and is at the center of the subtropical karst region in East Asia. Its climate is under the influence of EAM and IDM; the wet season starts in May and ends in October. The annual precipitation averages about 1400 mm, and the mean annual temperature is 19–20 °C. The 300 m-long Golden Lion Cave, located in south Libo County (25°7′-39′N, 108°37′–18′E), has well-developed speleothem deposits. The Dragon Spring Cave is located in north Libo County. It is 1.3 km in length and 3–80 m in height, and has abundant collapsed material to develop cave sediments. The two caves are close to the Dongge Cave (25°17′N, 108°5′E) whose speleothem $\delta^{18}O$ records for the past 150 kyr have been well studied (Yuan et al., 2004; Dykoski et al., 2005; Wang et al., 2005; Kelly et al., 2006). Since all three caves are located in the same sedimentary basin and have the same meteoric water source, their isotope records can be meaningfully compared with each other.

3. Samples and analytical methods

3.1. Stalagmites

Stalagmite L12, about 7 cm long, was collected from Dragon Spring Cave in 1998 (Fig. 2a). It can be divided into three sections: top to 25 mm is clean and composed of clear calcite crystals; 25–35 mm is brownish containing a fair amount of detritus; and 35–70 mm is like the first section with clear calcite crystals. There is a noticeable growth hiatus between the first and second sections (Fig. 2a). Stalagmites JSD-01 and JSD-02 were collected from Golden Lion Cave in 2006, each about 14 cm in length (Fig. 2b and c). Judging from the appearance and sedimentary characteristics, JSD-01 and JSD-02 should be two different parts of one broken stalagmite. Folded layering textures are seen along the growth axis at the center part of the stalagmites. In the outer part, growth layers parallel to the central main growth axis can also be readily identified (Fig. 2b and c). The mineral composition of the stalagmites is calcite.

3.2. ^{230}Th dating

From top to bottom of L12, 14 samples were collected along the growth axis (Fig. 2a). JSD-01 and JSD-02 were each sampled at the top (samples A9 and A7, respectively) and at the bottom (A10 and A8, respectively) parts along their growth axes (Fig. 2b and c). Additional two samples of JSD-02 were retrieved from growth layers parallel to the growth axis: one farther from the growth axis (A5) and the other closer to the growth axis (A6) (Fig. 2c). The sample sizes were about 100–300 mg; they were in powder form drilled using a micro-mill from the sectioned surfaces shown in Fig. 2. The dating was performed at the High-precision Mass Spectrometry and Environment Change Laboratory (HISPEC) of the National Taiwan University. Analyses of the U and Th isotopes followed the chemistry procedures of Shen et al. (2003). Instrumental analyses were performed using an inductively coupled plasma sector field mass spectrometer (ICP–SF-MS) (Shen et al., 2002), Thermo Finnigan Element II, and a multi-collector ICP–MS (MC-ICP–MS) (Frohlich et al., 2009), Neptune. Offline data reduction and calculations of U–Th isotopic compositions and concentrations, and ^{230}Th age were described in Shen et al. (2008). Table 1 lists the analytical and dating results.

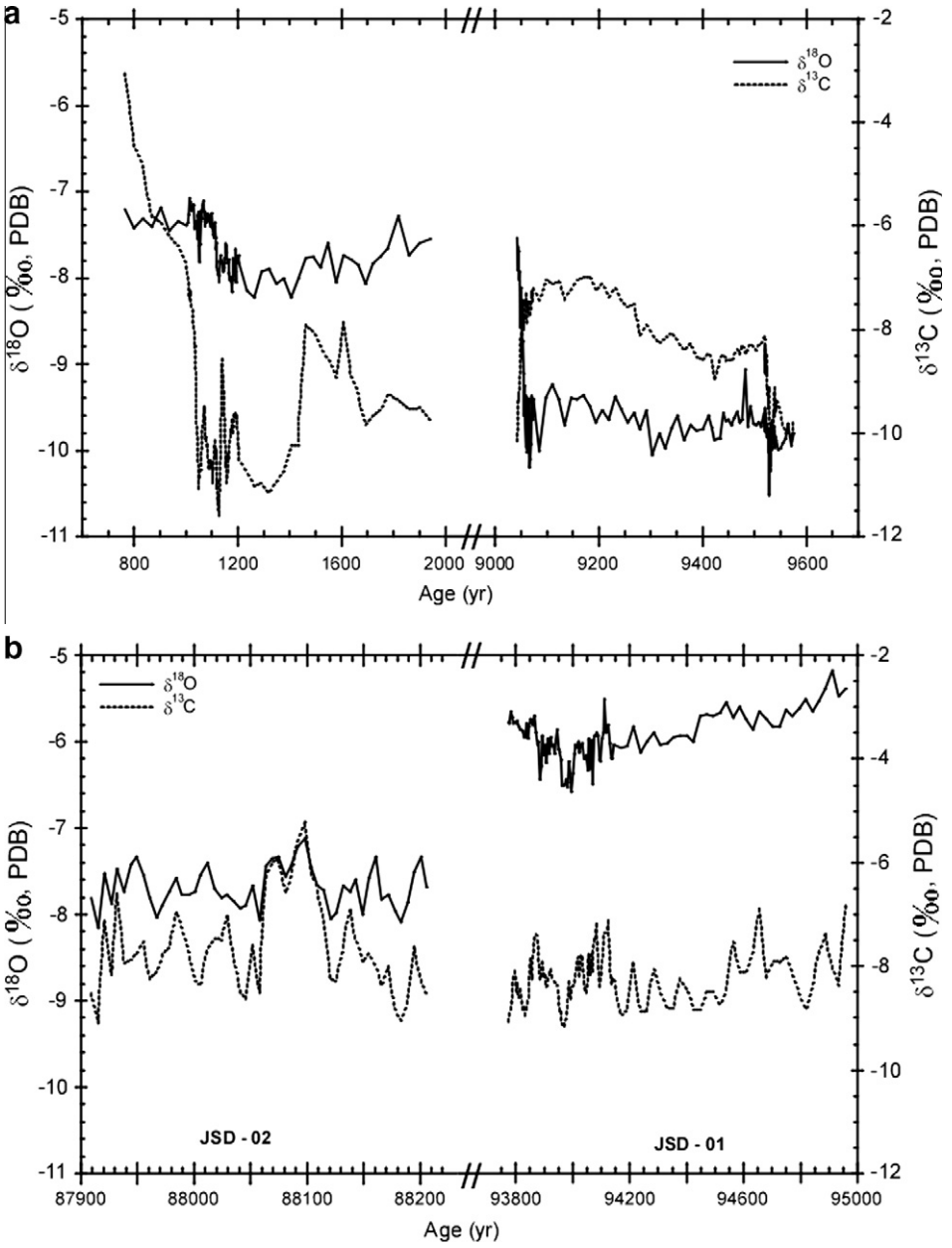

Fig. 3. The $\delta^{18}O$ and $\delta^{13}C$ records of the studied stalagmites. (a) The $\delta^{18}O$ and $\delta^{13}C$ records of L12 covering two periods: 870–1940 yr and 9045–9560 yr. (b) The $\delta^{18}O$ and $\delta^{13}C$ records of JSD-01 and JSD-02 covering two periods: 93,920–94,900 yr and 87,940–88,200 yr, respectively. The dotted lines denote $\delta^{13}C$ and the solid lines denote $\delta^{18}O$.

3.3. Stable isotope analysis

From the same sectioned surfaces sampled for ^{230}Th dating described above, we collected 283 micro-mill drilled powder subsamples from L12 at intervals of 0.25 mm/sample from top downward along the main growth axis, 258 subsamples from JSD-01 and 265 subsamples from JSD-02, both at intervals of 0.5 mm/sample. All of the 283 subsamples of L12 were analyzed for $\delta^{18}O$ and $\delta^{13}C$. For JSD-01 we analyzed each of the subsamples from top to 40 mm and then one out of every five subsamples below 40 mm (i.e., resolution = 2.5 mm). For JSD-02, we analyzed one out of every five subsamples throughout the entire specimen (i.e., resolution = 2.5 mm). Thus a total of 169 subsamples were analyzed for JSD-01 and JSD-02. Stable isotopic analyses were done using the Isotope Ratio Mass Spectrometry (IRMS) facility (Finnigan Kiel Carbonate Device III & Finnigan Delta plus XP) housed in the Earth Sciences Department of the National Cheng Kung University (NCKU). The calcite powders were dissolved at 70 °C in H_3PO_4. For quality control, a working standard was analyzed after each 10-sample runs. Repeated analyses ($N = 532$) of the NBS-19 standard gave $1.944 \pm 0.031‰$ for $\delta^{13}C$ and $-2.179 \pm 0.067‰$ for $\delta^{18}O$. All data are referred to PDB at 25 °C.

4. Results and discussion

4.1. Chronology

L12 was dated in two sequences (series A and V; Table 1) at different times. The results showed that the stalagmite grew in two periods during the Holocene: 870–1940 yr and 9045–9560 yr, separated by a growth hiatus (Fig. 2a). A plot of age vs. depth for the two growth periods gives average growth rates (i.e., linear fits) of 0.04 mm/yr and 0.077 mm/yr for the periods 870–1940 yr, and

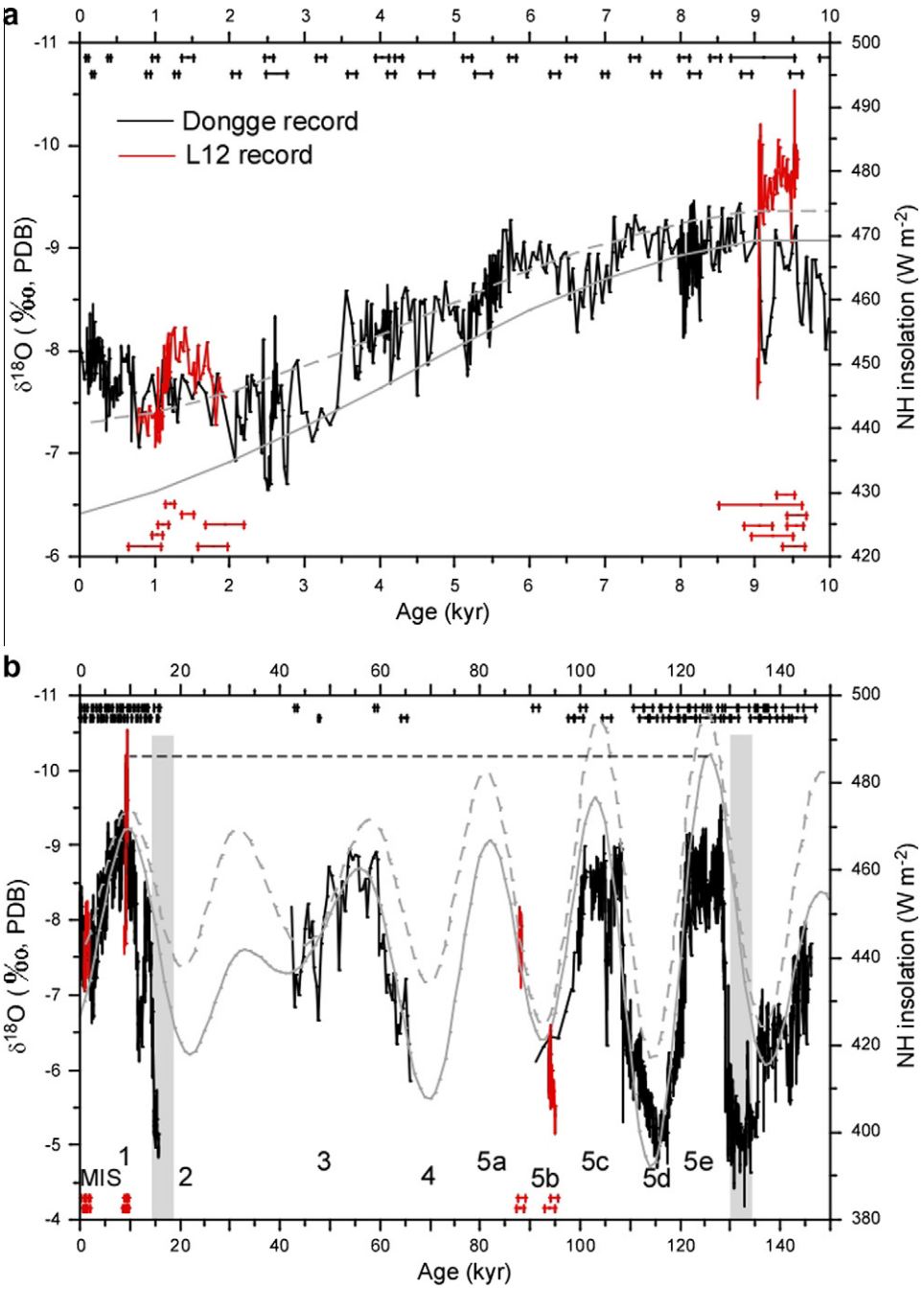

Fig. 4. Comparison of the $\delta^{18}O$ records of L12, JSD-01 and JSD-02 (red solid line) with the D3 and D4 $\delta^{18}O$ records of Dongge Cave (black solid line) and the NH solar insolation curves at 15°N (gray dotted line) and at 65°N (gray solid line). The ^{230}Th dates of the speleothem records are marked as red (this study) and black (Dongge records) horizontal bars. (a) Comparison for the Holocene period only. (b) Comparison over the past 150 kyr. Two vertical gray bars denote Terminations I and II, where the $\delta^{18}O$ records lag solar insolation by at least 5 kyr (see text for discussion and references).

9045–9560 yr, respectively. The age of sample V7 was not used in the plot as it has too large an error because of the high thorium content. The age–depth relationships thus deduced are used to establish the $\delta^{18}O$ and $\delta^{13}C$ records as shown in Fig. 3a.

The growth of JSD-01 and JSD-02 took place 93,920–94,900 yr and 87,940–88,200 yr, respectively, during the interval of Marine Isotope Stages (MIS) 5b–5a (Fig. 2b and c). Rapid growth of the two stalagmites results in the very short time intervals as observed, deterring us from carrying out further dating within the intervals to gain more detailed age controls. The ages for the $\delta^{18}O$ and $\delta^{13}C$ records are based on interpolation, assuming linear growth rates between the two ages obtained for each of the two stalagmites (Fig. 3b).

4.2. The $\delta^{13}C$ and $\delta^{18}O$ records

Fig. 3a shows that during 870–1940 yr, $\delta^{13}C$ in L12 fluctuated in the range of −3.06‰ to −11.61‰, and during 9045–9560 yr, the corresponding values were −6.98‰ to −10.75‰. Before AD 1000 and extending back to early Holocene, $\delta^{13}C$ was lighter than −5‰. Taking speleothem $\delta^{13}C$ records to reflect surface distribution of plants (Li et al., 1997; Ku and Li, 1998; Paulsen et al.,

2003), we see that after AD 1000 (i.e., since 1000 yr) the L12 $\delta^{13}C$ record clearly showed a rise toward heavy values reflecting a continuous and sharp decline of plant coverage above the Dragon Spring Cave. As the population of Guizhou experienced large influxes around the beginning of the South Song Dynasty (AD 1127) (Ge, 2005), the decline of plant coverage could be related to human activities (Chung, 2009; Kuo et al., this issue).

The pre-AD 1000 $\delta^{13}C$ values of lighter than −5‰ are further seen in the MIS 5 records of the two stalagmites from Golden Lion Cave. In JSD-01 (93,920–94,900 yr) and JSD-02 (87,940–88,200 yr), the $\delta^{13}C$ show ranges of −6.83‰ to −9.20‰ and −5.19‰ to −9.10‰, and mean values of −8.23‰ and −7.60‰, respectively (Fig. 3b).

The $\delta^{18}O$ in L12 shows much lighter signals (averaging −9.74‰) in early Holocene (9045–9560 yr) than those (averaging −7.63‰) in late Holocene (870–1940 yr) (Fig. 3a). This enrichment trend of $\delta^{18}O$ from early to late Holocene has been found in many other speleothem records and is thought to reflect a weakening of the summer monsoon resulting from solar insolation decrease (Fleitmann et al., 2003; Wang et al., 2005; Asmerom et al., 2007; Cosford et al., 2008; Hu et al., 2008). However, as speleothem $\delta^{18}O$ may register changes in local precipitation (Li et al., 1998), or vapor source (Fleitmann et al., 2003), or the total rainout along the vapor transport pathway (Hu et al., 2008), it remains to be explained as to why similar $\delta^{18}O$ records on millennium or longer time scales are found at different locations. If one interpreted the $\delta^{18}O$ records as proxy of rainfall amount, the similar $\delta^{18}O$ trends over monsoonal region of China during the Holocene would imply that the entire eastern China was wetter in early Holocene than in late Holocene. In fact, summer rainfall over eastern China has strongly spatial variability, and relationship between rainfall and monsoonal strength is also locality-dependent (Zhang et al., 2010). According to instrumental and historic records, contrast wetness condition in different parts of eastern China on decadal or longer time scales are quite normal. In addition, as the monsoonal frontal shifting toward to southeast with the solar insolation decrease, the maximum moisture in different areas over eastern China reached at different periods, being early Holocene in north China, and late Holocene in south China (An, 2000). Thus, if the similarity of the speleothem $\delta^{18}O$ trends represents changes in summer monsoon strength but not in rainfall amount, what is the physical meaning of the speleothem $\delta^{18}O$? This question needs to be further investigated.

$\delta^{18}O$ in JSD-01 varied between −5.17‰ and −6.58‰, averaging −5.95‰ over the period of 93,920–94,900 yr. In JSD-02, it varied between −7.12 and −8.16‰, averaging −7.68‰ over the interval of 87,940–88,200 yr (Fig. 3b). The two growth periods were at the transition from MIS 5b to MIS 5a, during which the speleothem $\delta^{18}O$ values depleted about 1.8‰, suggesting an enhancement of summer monsoon and precipitation. In what follows, we will compare the summer monsoon strengths during MIS 5b–5a and early/late Holocene in China.

4.3. Comparison of stalagmite $\delta^{18}O$ records in Libo area

As proxy for climate changes $\delta^{18}O$ in speleothem is required to be in isotopic equilibrium with the mother solution from which the calcite precipitates. Hendy (1971) has discussed ways to fulfill or check for the equilibrium requirement, including selecting stalagmite samples from deep parts of caves where humidity is high. In this study, all three stalagmites were carried out Hendy Test, showing no kinetic effect in isotopic equilibrium during the calcite precipitation. More ever, an effective way of ensuring isotopic equilibrium would be the reproducible $\delta^{18}O$ records obtained on different speleothems from the same cave or from caves in the same general area. Good reproducibility should give confidence to our interpreting the $\delta^{18}O$ signals as a reflection of climate change; i.e., the signals are free of non-equilibrium isotopic fractionation.

Fig. 4 shows the matching of $\delta^{18}O$ records for several speleothems collected from three caves in the Libo County. In Fig. 4a are plotted the high-resolution (centennial scale) speleothem $\delta^{18}O$ data obtained from Dragon Spring Cave (stalagmite L12; this study) and Dongge Cave (stalagmite D4; Dykoski et al., 2005), together with the summer insolation variations at 15°N and 65°N for the past 10 kyr (Berger and Loutre, 1991). Similar comparison plots are shown in Fig. 4b, where the $\delta^{18}O$ data of Golden Lion Cave (stalagmites JSD-01 and JSD-02; this study) and the Dongge Cave (stalagmites D3 and D4; Yuan et al., 2004; Dykoski et al., 2005; Kelly et al., 2006) are plotted, together with the 15°N and 65°N insolation curves.

The matching is good both between the $\delta^{18}O$ records of L12 and D4 (Fig. 4a) and those between JSD-01 and D3 (Fig. 4b). The L12–D4 matching shows a ~0.5‰ difference in the absolute $\delta^{18}O$ value. However, the difference is acceptable considering errors involved in the dating and possible differences in cave temperature and drip-water source for the two records, not to mention the fact that a similar offset has also been noted in the two Dongge Cave records of DA and D4 (Yuan et al., 2004; Dykoski et al., 2005; Wang et al., 2005). The compatible $\delta^{18}O$ records of the Libo County speleothems serve to demonstrate the value of such records in climate reconstruction.

The JSD-02 record of 87,940–88,200 yr may be taken to fill a part of the void left in the Dongge record. This thinking stems from the observation that the Libo County speleothem $\delta^{18}O$ records and NH summer solar-insolation variations assume a similar trend in that lightening of speleothem $\delta^{18}O$ is coupled to the increasing summer insolation (Fig. 4a and b). The coupling of the two trends offers a means of retracing the millennial variation of EASM over the past 150 kyr.

The speleothem $\delta^{18}O$–solar insolation relationship shown in Fig. 4 also reveals several unexplained features about the EASM. These include: (1) during the past 150 kyr, the strongest solar insolation occurred in MIS 5e (ca. 125 ka), whereas the strongest summer monsoon, as indicated by the lightest speleothem $\delta^{18}O$, occurred in early Holocene; (2) at glacial–interglacial transition times of Termination II (134–129 ka) and Termination I (18–14 ka), the increase of insolation led the decrease of speleothem $\delta^{18}O$, hence the intensification of EASM, by 5 kyr or more; and (3) loess sequence, marine-sediments and ice cores all show that global climate during MIS 5d and 5e was milder than during glacial periods and even the late Holocene. But this is not reconciled by the Fig. 4b data, which show that MIS 5d had the lowest insolation intensity and heaviest speleothem $\delta^{18}O$.

5. Comparison of speleothem $\delta^{18}O$ records with other global records

Precisely dated, high-resolution speleothem $\delta^{18}O$ records from eastern China, notably those from Dongge Cave (25°17′N, 108°5′E), Hulu Cave (32°30′N, 119°10′E), and Sanbao Cave (31°40′N, 110°26′E), have become available. These three caves are all located in the subtropical monsoon regions with vapor sources mainly brought in by the EASM from the equatorial Pacific Ocean. Summer rainfall supplies more than 80% of the annual precipitation. Their $\delta^{18}O$ records have been used to reconstruct the variability of EASM over the past 220 kyr, on the time scale of earth's orbital changes (Wang et al., 2001, 2008; Yuan et al., 2004; Dykoski et al., 2005; Cheng et al., 2006; Kelly et al., 2006). Of particular interest concerning those records is that they show $\delta^{18}O$ variations coincident with the 23-kyr precession cycles (Fig. 5c–e). What causes the coincidence is a question waiting to be answered. To search for the answer,

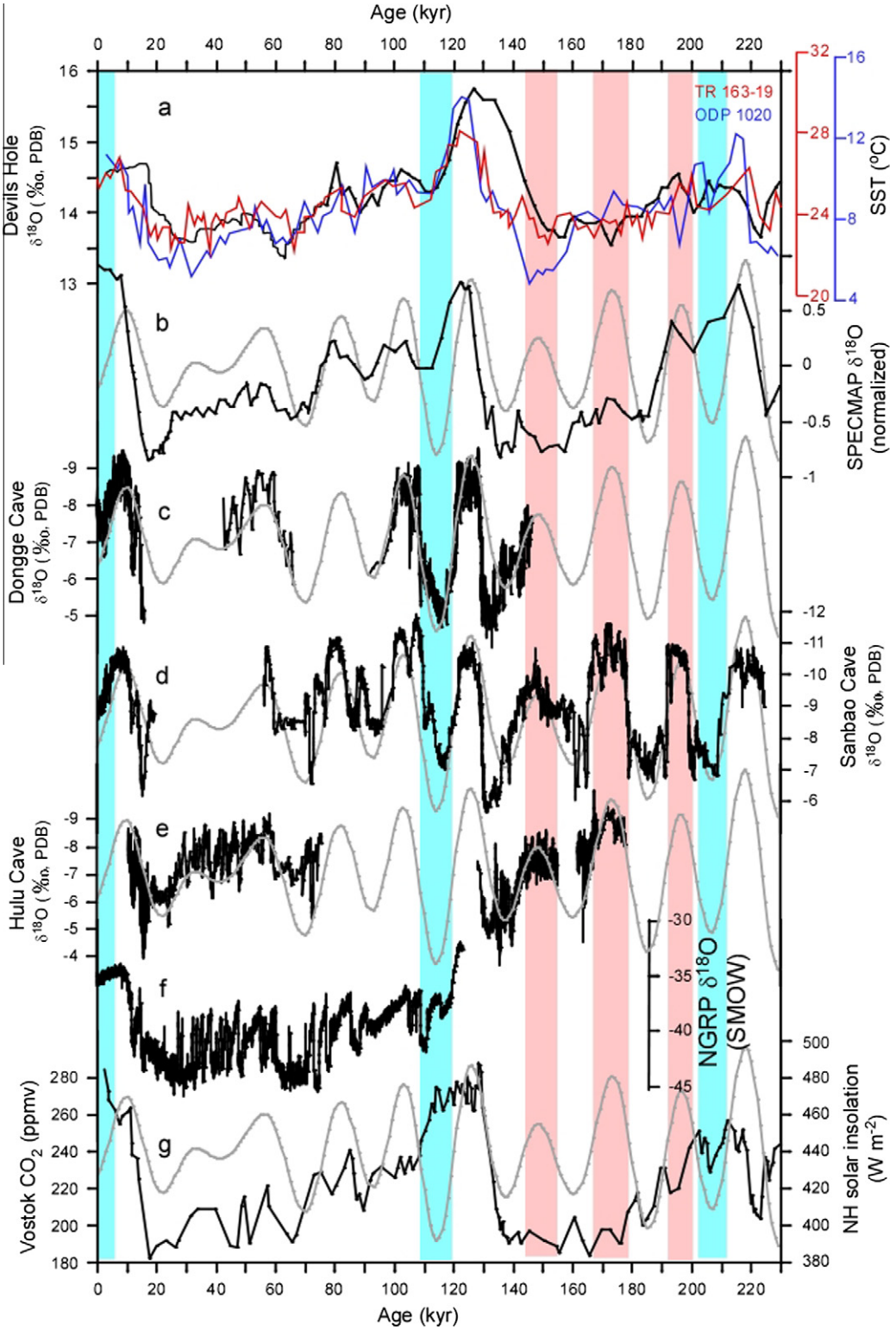

Fig. 5. Comparisons among the Chinese speleothem $\delta^{18}O$ records, NH solar insolation at 65°N (gray solid line), and other global climatic records during the past 230 kyr. (a) Devils Hole calcite-vein $\delta^{18}O$ record (black line), SST variations in the equator Pacific Ocean (red line) and off the California coast (blue line); (b) SPECMAP; (c) Dongge $\delta^{18}O$ records; (d) Sanbao $\delta^{18}O$ records; (e) Hulu $\delta^{18}O$ records; (f) $\delta^{18}O$ records in NGRIP ice core; and (g) CO_2 records in Vostok ice core. Glacial periods including MIS 2, 3, 4 and 6 are remarked in blue color (see text for discussion and references).

we begin by comparing, in addition to the three cave (i.e., EASM) records mentioned above, a variety of other marine and terrestrial records bearing global climatic information with the NH solar insolation curve constructed for the 65° latitude (Berger and Loutre, 1991). The comparisons are shown in Fig. 5, in which superimposed on the insolation curve for the last 230 kyr are the following records: (1) Devils Hole calcite-vein $\delta^{18}O$ record depicting the variation of vapor sources from the tropics and subtropics (Winogard et al., 1992,

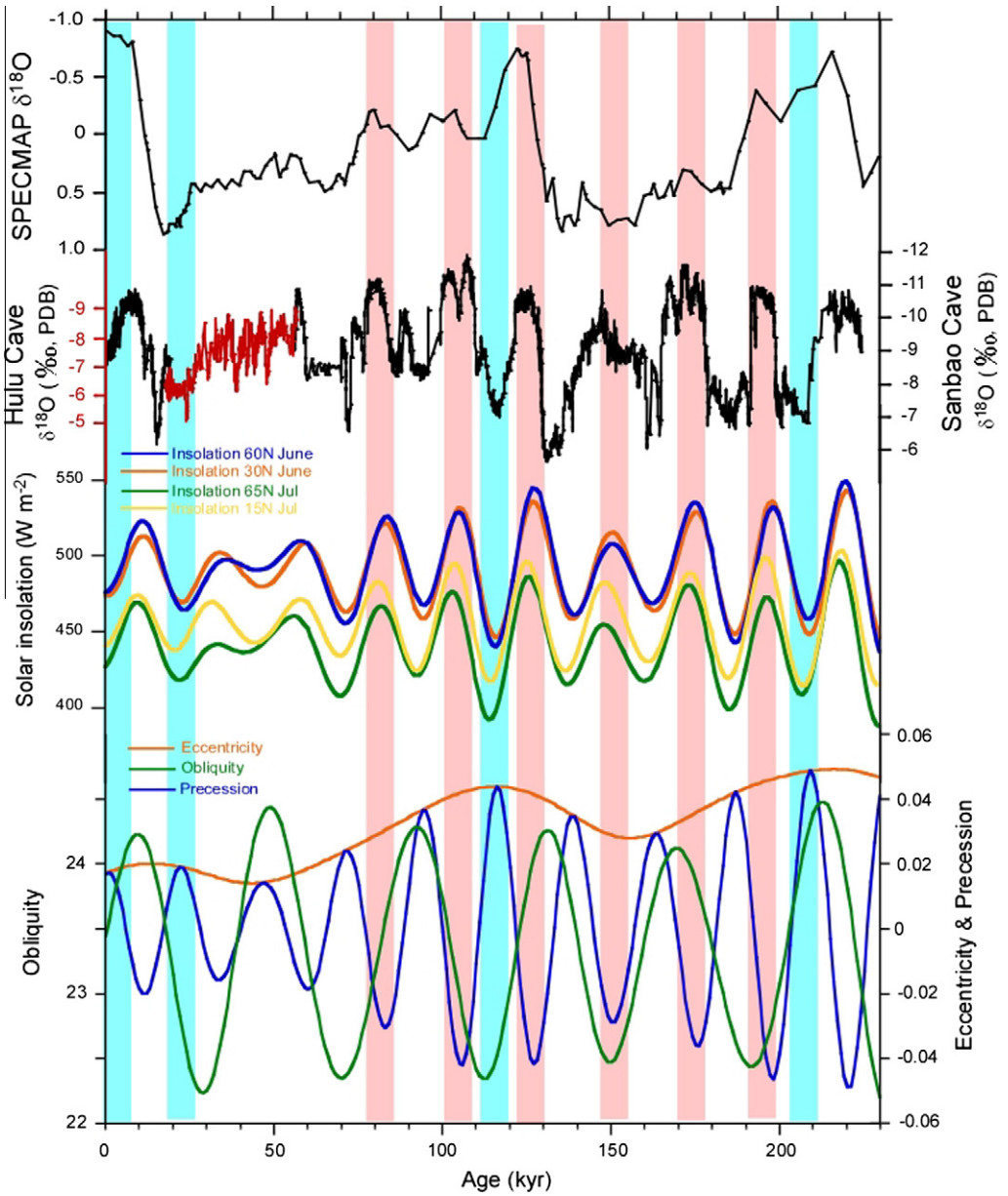

Fig. 6. Comparisons among SPCEMAP record, the Chinese speleothem $\delta^{18}O$ records including Sanbao records (black) and Hulu records (red), NH solar insolations at various latitudes in summer months, and orbital variations including eccentricity (orange), obliquity (green) and precession (blue). Turquoise areas denote glacial periods (see text for discussion and references).

1997, 2006; Winogard, 2002); (2) sediment records depicting sea surface temperature (SST) variations in the equator Pacific Ocean (core TR 163-19) and the California coast (ODP 1020) (Lea et al., 2000; Herbert et al., 2001); (3) SPECMAP depicting the sea level or ice volume changes (Fig. 5b) (Martinson et al., 1987); (4) speleothem $\delta^{18}O$ records from Dongge, Sanbao, and Hulu Caves depicting the variations about the EASM and precipitation (Fig. 5c–e) (Wang et al., 2001, 2008; Yuan et al., 2004; Dykoski et al., 2005; Kelly et al., 2006); (5) $\delta^{18}O$ records in ice core NGRIP depicting air temperature variations in Greenland (Fig. 5f) (North Greenland Ice-Core Project Members, 2004); and (6) CO_2 records in Vostok ice core depicting air temperature variations in the Antarctica (Fig. 5g) (Petit et al., 1999).

Fig. 5 shows that speleothem $\delta^{18}O$ records from the monsoon area of eastern China are distinctly different from the other records. The most salient distinction is that the speleothem $\delta^{18}O$ mimics well the ~23-kyr precession cycles of the solar insolation, whereas all the other records are primarily modulated by the ~100-kyr eccentricity cycles of the solar insolation; their modulation by the precession is faint at best. There are other notable differences: (1) SPECMAP and Vostok records during MIS 1 (Holocene) do not follow the solar insolation curve which dropped significantly from early Holocene to late Holocene; (2) speleothem and solar insolation records indicate that EASM during MIS 5b, 5d and late Holocene could be weaker than during glacial periods (e.g., MIS 6). This appears to contradict the other records showing that throughout MIS 5 climate was warm and warmer than that of MIS 2, 4 and 6; and (3) within the two penultimate interglacial periods MIS 5 and 7 (e.g., 110–120 ka, 200–220 ka), records other than those of speleothem $\delta^{18}O$ show either phase legs or no correlation with insolation.

Explaining the differences cited above should help understand climate variations in the past. It has been thought (Milankovitch, 1941) that earth's glacial–interglacial successions are related to

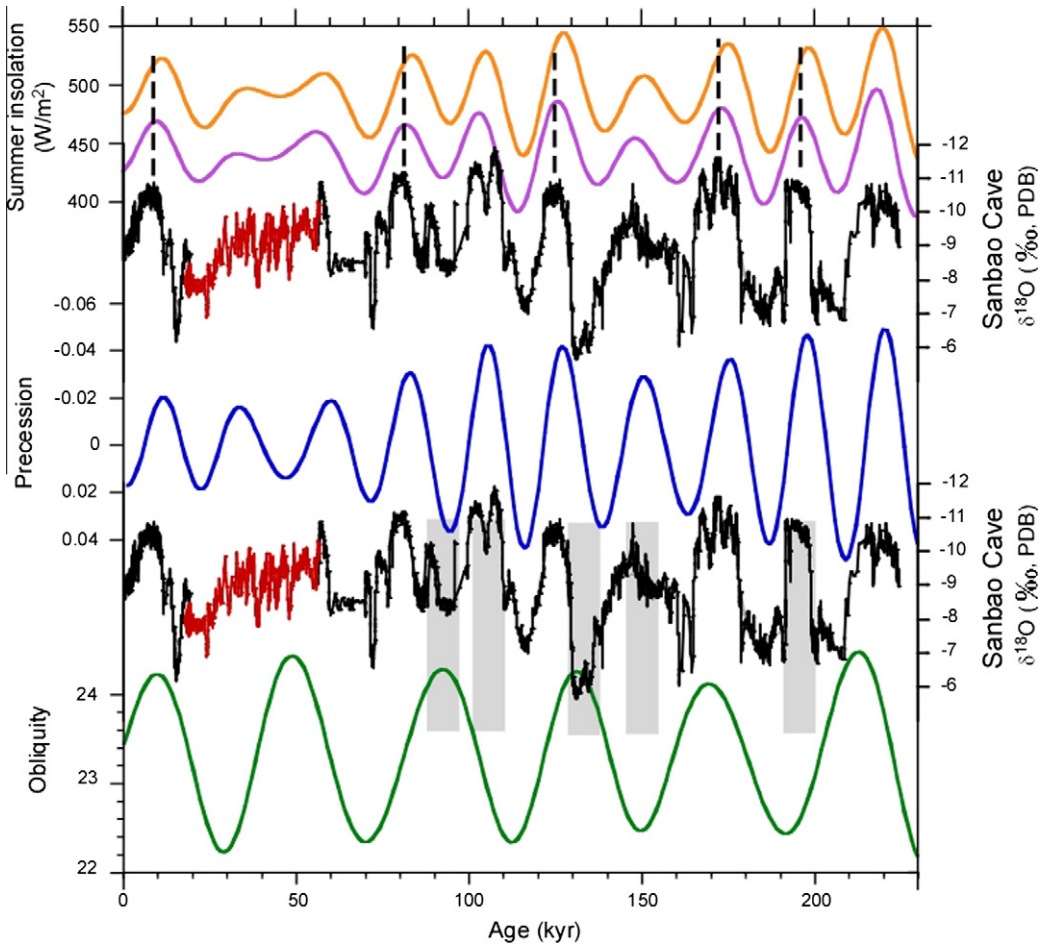

Fig. 7. Detailed comparison of the Sanbao records (black) and Hulu records (red part) with the NH solar insolation at 60°N in June (orange) and at 65°N in July (purple), and with obliquity (green) and precession (blue). Note that the Hulu records have different scale for $\delta^{18}O$ values as for the Sanbao records (see Fig. 6). Gray bars denote the contradicting intervals of the $\delta^{18}O$ records against obliquity cycles. The vertical dashed lines indicate time offsets between the June and July insolation curves.

the orbital movement of the planet, in that solar insolation reflects the combined effects of three orbital elements: eccentricity, obliquity and precession, each having its own cyclicity (Liu, 1999; Imbrie and Imbrie, 1980). As mentioned, glacial–interglacial cycles as delineated by SST, $\delta^{18}O$ in vapor source from tropical-subtropical areas, sea level (ice volume), and air temperature and CO_2 concentration, are mainly in tune with the ~100 kyr eccentricity cycle that overrides on the obliquity (~41-kyr period) and precession (~23-kyr period) cycles (Fig. 5). Low eccentricity corresponds to glacial periods, and high eccentricity to interglacial periods (Fig. 6). In contrast, the speleothem $\delta^{18}O$ records in eastern China are chiefly steered by insolation's precession component which varies with a cyclicity of ~23 kyr.

However, this precession-modulated insolation is seen not to affect terrestrial $\delta^{18}O$ records outside of monsoonal area, such as those from the Devils Hole (Winogard et al., 2006), Soreq Cave and Peqiin Cave (Bar-Matthews et al., 2003). Instead, these records match the SST variations derived from marine cores, which reflect glacial–interglacial cycling, or insolation cycles due to eccentricity change. Furthermore, it is noteworthy that subtropical Brazilian caves yield $\delta^{18}O$ records reflecting monsoon variations paced by the SH summer solar insolation, which, on sub-millennial scales, has an anti-phasing relationship with the NH summer insolation (Cruz et al., 2005, 2006; Wang et al., 2006). Clemens (2007), in summarizing the long-term variability of Asian Monsoon reconstructed by paleoclimatic records, noted that earth-orbital periods associated with precession of the equinoxes and obliquity of the Earth's axis dominate the insolation and summer monsoon spectra whereas the 100-kyr variance associated with the great ice ages dominates the winter monsoon variability. An et al. (2001) deduced from the Chinese loess-soil sequence of the past 2.6 Myr that within the interval of the large amplitude 100-kyr ice age cycles, the summer and winter monsoon proxies of Asian Monsoon are out of phase with stronger winter monsoons and weaker summer monsoons during glacial intervals, and stronger summer monsoons and weaker winter monsoons during interglacial intervals. The in-phase relationship of strong winter monsoon with maximum ice volume at the 100-kyr band has also been found in marine records which also reflected the EASM (e.g., Beaufort et al., 2003; Wei et al., 2003). However, these "winter monsoon" records show phase lags with the obliquity band and have very little 23-kyr amplitude (Beaufort et al., 2003; Clemens, 2007).

To summarize, the Chinese speleothem $\delta^{18}O$ records reveal strong in-phase relationship with NH solar insolation. Maximum EASM corresponds to NH summer solar insolation maxima (maximum obliquity and minimum precession; June 21 perihelion), which strongly influence the sensible heating of the Tibetan Plateau (An et al., 2001; Prell and Kutzbach, 1987, 1992). Stronger NH summer insolation would export more latent heat from the southern Indian Ocean to Asia (Clemens, 2007), perhaps resulting in stronger EASM. However, this solar forcing at the 23-kyr band is not the cause for the 100-kyr cycle global climates which include

changes in global ice volume, sea level, SST, atmospheric CO_2, and loess accumulation. Therefore, caution should be used in comparing the speleothem records with other climatic proxies on 10^4–10^5-yr scales.

Because the 23-kyr and 41-kyr Earth-orbital cycles have large amplitude variation (by the order of 10% relative to the present level) and the 100-kyr eccentricity cycle has very small variation (only 0.1% of the present level) (Beer et al., 2000; Imbrie et al., 1993; Solanki, 2002; Soon et al., 2000), the 100-kyr cycle Pleistocene ice age dominated global climates are not explained by these orbital radiation cycles. Up-to-date, however, there is no good explanation for the influence of climatic feedback mechanisms internal to the climate system (Clemens, 2007). Nevertheless, from Figs. 5 to 6 one can see that many global climate proxies show the 100-kyr glacial/interglacial cycles probably driven by the orbital eccentricity component. As the stalagmite records from monsoonal regions reflect the monsoonal precipitation that is more influenced by the thermal heating following the precessional forcing, one may expect that they are different from the non-monsoonal records about the 100-kyr climatic cycles because the later records may be more influenced by the obliquity-related feedbacks. It has been noted that the 100-kyr climatic cycles may be a non-linear response to orbital obliquity while eccentricity somehow still plays a "pacing" role (Huybers and Wunsch, 2005; Huybers, 2006; Liu et al., 2008).

6. Influence of solar insolation on EASM

Although the NH summer solar insolation driven by the 23-kyr and 41-kyr Earth-orbital cycles may be the main controlling factor of the EASM variability on 10^4–10^5-yr scales, Fig. 6 shows that the 41-kyr obliquity band is weak in both the insolation curves and the $\delta^{18}O$ records. We further compare the $\delta^{18}O$ records with obliquity and precession as well as with the summer solar insolation in June and July (Fig. 7). In many intervals, the light $\delta^{18}O$ (strong EASM) corresponds to minimum obliquity and heavy $\delta^{18}O$ (weak EASM) correspond to maximum obliquity (gray bars in Fig. 7). The correspondence is at odd with the aforementioned correspondence of EASM maxima with maximum obliquity and minimum precession (Clemens, 2007 and references therein). Rather, the $\delta^{18}O$ records mimic the precession curve well (Fig. 7). Orbital precession affects seasonality of the Earth's climate especially the wet/dry season changes in low latitude areas where the seasonality is chiefly reflected by wet vs. dry months. Hence, we may hypothesize that when solar radiation increases in the northern hemisphere at low precession, an increased north–south thermal gradient of the troposphere causes a northward movement of ITCZ. This northward-shift of ITCZ brings about heavy convective precipitation over eastern China (Wang, 2007) and leads to an earlier starting date and longer duration of EASM over eastern China. As a consequence, increasing the total amount of monsoonal rain and/or the summer/winter precipitation ratio will give rise to light speleothem $\delta^{18}O$. Therefore, variability of the EASM intensity on 10^4–10^5-yr scales is mainly controlled by the orbital precession-driven 23-kyr solar insolation. It is also interesting to note that the $\delta^{18}O$ records match the solar insolation curve in July better than in June (Fig. 7). This means that, rather than corresponding to minimum precession at June 21 perihelion, the EASM maxima may correspond to mid-to-late summer insolation.

7. Conclusions

1. Four $\delta^{18}O$ records in three stalagmites from the Dragon Spring and Golden Lion Caves located in Libo County of Guizhou, China indicate that the EASM intensity was stronger in 9–9.6 ka (early Holocene) than in 0.75–2 ka (late Holocene). Strengthening of EASM occurred from 93.8–95.2 ka to 87.9–88.2 ka during MIS 5b–5a.
2. The four records fit well with the published Dongge Cave record from the same area, reinforcing the role of stalagmite $\delta^{18}O$ as a proxy for the regional precipitation or strength of the East Asian Monsoon.
3. On suborbital scales, the stalagmite $\delta^{18}O$ records exhibit many discrepancies with variations of the NH summer solar insolation. For instance, the increase of solar insolation at Termination II and Termination I led the decrease of speleothem $\delta^{18}O$ by at least 5 kyr. The opposite trends between the solar insolation and the $\delta^{18}O$ indicate that the EASM intensity was controlled by the external forcing during these intervals. It is important to understand these discrepancies for paleoclimate study.
4. Comparison of stalagmite $\delta^{18}O$ records from Dongge, Sanbao and Hulu Caves with solar insolation and other global climate records during the past 230 kyr on 10^4–10^5-yr scales, reveals that: (a) the $\delta^{18}O$ records resemble well the NH summer solar insolation which is primarily driven by Earth's orbital precession with a 23-kyr cycle. (b) The $\delta^{18}O$ records do not match the obliquity and eccentricity cycles, whereas the 100-kyr cycles are pervasive in other paleoclimate records depicting changes in global ice volume, sea level, SST, atmospheric CO_2, and loess accumulation. As the 100-kyr eccentricity cycle seems too small to explain the ice volume change between the glacial and interglacial intervals, the internal forcing mechanism remains unclear. (c) The 23-kyr cycle of EASM intensity changes can be attributed to forcing by precession changes, which govern the distribution of solar radiation in northern and southern hemispheres, and the shift of the ITCZ and the average frontal positions of monsoons. Stronger NH hemisphere radiation leads to stronger EASM, more monsoon rains, higher ratio of summer/winter precipitation, and lighter $\delta^{18}O$ in stalagmites from monsoonal regions. (d) The discrepancy between the Chinese speleothem $\delta^{18}O$ records with 23-kyr cycles and the global ice-volume-controlled climate proxies with 100-kyr cycles calls for a better understanding of the relationship between the Asian Summer Monsoon and winter monsoon, as well as of the correlation between maritime and terrestrial summer monsoon proxies.

Acknowledgement

Funding for this study was provided by the Science Council of Taiwan (NSC 97-2628-M-006-014 and 98-2116-M-006 -003), the National Natural Science Foundation of China (Grant No. 40672202) and Special research grant for Academician from Chongqing Science and Technology Commission (Grant No. 20037835). Funding for ^{230}Th dating at the HISPEC was supported by the NSC Grants (98-2116-M-002-012 and 98-2611-M-0092-006 to CCS). We thank two anonymous reviewers for their constructive and useful comments.

References

An, Z., Kutzbach, J.E., Prell, W.L., Porter, S.C., 2001. Evolution of Asian monsoons and phased uplift of the Himalaya–Tibetan plateau since Late Miocene times. Nature 411, 62–66.

An, Z., 2000. The history and variability of the East Asian paleomonsoon climate. Quaternary Science Reviews 19, 171–187.

Asmerom, Y., Polyak, V., Burns, S., Rassmussen, J., 2007. Solar forcing of Holocene climate: new insights from a speleothem record, southwestern United States. Geology 35, 1–4.

Bar-Matthews, M., Ayalon, A., Gilmour, M., Matthews, A., Hawkesworth, C.J., 2003. Sea–land oxygen isotopic relationships from planktonic foraminifera and

speleothems in the Eastern Mediterranean region and their implication for paleorainfall during interglacial intervals. Geochimica et Cosmochimica Acta 67, 3181–3199.
Beaufort, L., de Garidel-Thoron, T., Linsley, B., Oppo, D., Buchet, N., 2003. Biomass burning and oceanic primary production estimates in the Sulu Sea area over the last 380 kyr and the East Asian monsoon dynamics. Marine Geology 201, 53–65.
Beer, J., Mende, W., Stellmacher, R., 2000. The role of the sun in climate forcing. Quaternary Science Reviews 19, 403–415.
Berger, A., Loutre, M.F., 1991. Insolation values for the climate of the last 10 million years. Quaternary Sciences Review 10, 297–317.
Broecker, W.S., 1994a. Is earth climate poised to jump again? Geotimes 39 (11), 16–18.
Broecker, W.S., 1994b. Massive iceberg discharges as triggers for global climate change. Nature 372, 421–424.
Burns, S.J., Fleitmann, D., Matter, A., Kramers, J., Al-Subbary, A.A., 2003. Indian Ocean climate and an absolute chronology over Dansgaard/Oeschger events 9 to 13. Science 301, 1365–1367.
Chen, L.X., Zhu, Q.G., Luo, H.B., He, J.H., Dong, M., Feng, Z.Q., 1991. The East Asian Monsoon. Meteorological Press, Beijing. pp. 304–346 (in Chinese).
Cheng, H., Edwards, R.L., Hoff, J., Gallup, C.D., Richards, D.A., Asmerom, Y., 2000. The half-lives of uranium-234 and thorium-230. Chemical Geology 169, 17–33.
Cheng, H., Edwards, R.L., Kong, X., Ming, Y., Kelly, M.J., Wang, X., Gallup, C.D., 2006. A penultimate glacial monsoon record from Hulu Cave and two-phase glacial terminations. Geology 34, 217–220.
Chung, W.L., 2009. The Late Quaternary Climate and Environmental Changes of the Southwest China: Stalagmite Carbon and Oxygen Isotope Records from Libo, Guizhou. M.Sc. Thesis, National Sun Yat-sen University, Taiwan, 76 p.
Clemens, S.C., Prell, W.L., 2007. The timing of orbital-scale Indian monsoon changes. Quaternary Science Reviews 26, 275–278.
Clemens, S.C., Prell, W.L., Murray, D., Shimmield, G., Weedon, G., 1991. Forcing mechanisms of the Indian Ocean monsoon. Nature 353, 720–725.
Clemens, S.C., 2007. Extending the historical record by proxy. In: Wang, B., (Ed.), Springer Praxis Publishing, Chichester, UK. ISBN 3-540-40610-7, pp. 615–630,787.
Cosford, J., Qing, H., Yuan, D., Zhang, M., Holmden, C., Patterson, W., Cheng, H., 2008. Millennial-scale variability in the Asian monsoon: evidence from oxygen isotope records from stalagmites in southeastern China. Palaeogeography, Palaeoclimatology, Palaeoecology 266, 3–12.
Cruz Jr., F.W., Burns, S.J., Karmann, I., Sharp, W.D., Vuille, M., Cardoso, A.O., Ferrari, J.A., Silva Dias, P.L., Viana Jr., O., 2005. Insolation-driven changes in atmospheric circulation over the past 116 kyr in subtropical Brazil. Nature 434, 63–66.
Cruz Jr., F.W., Burns, S.J., Karmann, I., Sharp, W.D., Vuille, M., 2006. Reconstruction of regional atmospheric circulation features during the Late Pleistocene in subtropical Brazil from oxygen isotope composition of speleothems. Earth and Planetary Science Letters 248, 494–506.
Ding, Z.L., Liu, T.S., Rutter, N.W., Yu, Z., Guo, Z., Zhu, R., 1995. Ice-volume forcing of East Asian winter monsoon variations in the past 800,000 years. Quaternary Research 44, 149–159.
Ding, Z.L., Derbysgier, E., Yang, S.L., Yu, Z.W., Xiong, S.F., Liu, T.S., 2002. Stacked 2.6-Ma grain size record from the Chinese loess based on five sections and correlation with the deep-sea $\delta^{18}O$ record. Paleoceanography 17, 5-1–5-21.
Dykoski, C.A., Edwards, L.R., Cheng, H., Yuan, D., Cai, Y., Zhang, M., Lin, Y., Qing, J., An, Z., Revenaugh, J., 2005. A high-resolution, absolute-dated Holocene and deglacial Asian monsoon record from Dongge Cave, China. Earth and Planetary Science Letters 233, 71–86.
Fleitmann, D., Burns, S., Mudelsee, M., Neff, U., Kramers, J., Mangini, A., Matter, A., 2003. Holocene forcing of the Indian monsoon recorded in a stalagmite from southern Oman. Science 300, 1737–1739.
Frohlich, C., Hornbach, M.J., Taylor, F.W., Shen, C.-C., Moala, A., Morton, A.E., Kruger, J., 2009. Huge erratic boulders in Tonga deposited by a prehistoric tsunami. Geology 37, 131–134.
Gao, Y.X., Xu, S.Y., 1962. Some Problems of East Asian Monsoon. Science Press, Beijing. pp. 1–49 (in Chinese).
Ge, J.X., 2005. Population History of China, vol. 6. Fudian University Press, Shanghai. pp. 3946 (in Chinese).
Hendy, C.H., 1971. The isotope geochemistry of speleothem: I. The calculation of the effects of different modes of formation on the isotopic composition of speleothems and their applicability as paleoclimatic indicators. Geochimica et Cosmochimica Acta 35, 801–824.
Herbert, T.D., Schuffert, J.D., Andreasen, D., Heusser, L., Lyle, M., Mix, A., Ravelo, A.C., Stott, L.D., Herguera, J.C., 2001. Collapse of the California current during glacial maxima linked to climate change on land. Science 293, 71–76.
Hu, C., Henderson, G.M., Huang, J., Xie, S., Sun, Y., Johnson, K.R., 2008. Quantification of Holocene Asian monsoon rainfall from spatially separated cave records. Earth and Planetary Science Letters 266, 221–232.
Huybers, P., Wunsch, C., 2005. Obliquity pacing of the late Pleistocene glacial terminations. Nature 434, 491–494.
Huybers, P., 2006. Early Pleistocene glacial cycles and the integrated summer insolation forcing. Science 313, 508–511.
Imbrie, J., Imbrie, J., 1980. Modeling the climatic response to orbital variations. Science 207, 943–953.
Imbrie, J., Berger, A., Boyle, E.A., Clemens, S.C., Duffy, A., Howard, W.R., Kukla, G., Kutzbach, J., Martinson, D.G., McIntyre, A., et al., 1993. On the structure and origin of major glaciation cycles. Part 2: the 100,000-year cycle. Paleoceanography 8, 699–735.
Johnson, K.R., Ingram, B.L., 2004. Spatial and temporal variability in the stable isotope systematics of modern precipitation in China: implications for paleoclimate reconstructions. Earth and Planetary Sciences Letters 220, 365–377.
Kelly, M.J., Edwards, R.L., Cheng, H., Yuan, D., Cai, Y., Zhang, M., Lin, Y., An, Z., 2006. High resolution characterization of Asian monsoon between 146,000 and 99,000 years B.P. from Dongge Cave, China and global correlation of events surrounding Termination II. Palaeogeography, Palaeoclimatology, Palaeoecology 236, 20–38.
Ku, T.-L., Li, H.-C., 1998. Speleothems as high-resolution paleoenvironment archives: records from northeastern China. Journal of Earth System Science 107, 321–330.
Kuo, T.S., Liu, Z.-Q., Li, H.-C., Wan, N., Shen, C.-C., Ku, T.-K., this issue. Climate and environmental changes during the past millennium in central western Guizhou, China as recorded by Stalagmite ZJD-21. Journal of Asian Earth Sciences.
Lea, D.W., Pak, D.K., Spero, H.J., 2000. Climate impact of late Quaternary equatorial Pacific sea surface temperature variations. Science 289, 1719–1724.
Li, H.C., Ku, T.L., Stott, L.D., Yuan, D., Chen, W., Li, T., 1997. Interannual-resolution $\delta^{13}C$ record of stalagmite as proxy for the change in precipitation and atmosphere CO_2 in Shihua Cave, Beijing. Carsologica Sinica 16, 285–295 (in Chinese).
Li, H.-C., Ku, T.-L., Stott, L.D., Chen, W.J., 1998. Applications of interannual – resolution stable isotope records of speleothem: climatic changes in Beijing and Tianjin, China during the past 500 years – the $\delta^{18}O$ record. Science in China 28, 181–186.
Li, H.-C., Ku, T.-L., You, C.F., Cheng, H., Edwards, R.L., Ma, Z.B., Tsai, W.S., Li, M.D., 2005. $^{87}Sr/^{86}Sr$ and Sr/Ca in speleothems for paleoclimate reconstruction in central China between 70 and 280 kyr ago. Geochimica et Cosmochimica Acta 69, 3933–3947.
Li, H.-C., Yuan, D.-X., Ku, T.-L., Wan, N.-J., Ma, Z.-B., Zhang, P.-Z., Bar-Matthews, M., Ayalon, A., Liu, Z.-H., Zhang, M.-L., Zhu, Z.-Y., Wang, R.-M., 2007. Stable isotopic compositions of waters in the karst environments of China: climatic implications. Applied Geochemistry 22, 1748–1763.
Liu, T.S., Ding, Z., Rutter, N., 1999. Comparison of Milankovitch periods between continental loess and deep sea records over the last 2.5 Ma. Quaternary Science Reviews 18, 1205–1212.
Liu, Z., Cleaveland, L.C., Herbert, T.D., 2008. Early onset and origin of 100-kyr cycles in Pleistocene tropical SST records. Earth and Planetary Science Letters 265, 703–715.
Liu, H., 1999. Insolation changes caused by combination of amplitude and frequency modulation of the obliquity. Journal of Geophysics Research 104, 25197–25206.
Martinson, D.G., Pisias, N.G., Hays, J.D., Imbrie, J., Moore, T.C., Shackleton, N.J., 1987. Age dating and the orbital theory of the ice ages: development of a high-resolution 0 to 300,000-year chronostratigraphy. Quaternary Research 27, 1–29.
Milankovitch, M.M., 1941. Canon of Insolation and the Ice Age Problem. Koniglich Serbische Akademie, Beograd (English translation by the Israel Program for Science Translations). Published for the US Department of Commerce and the National Science foundation, Washington, DC.
North Greenland Ice-Core Project (NorthGRIP) Members, 2004. High-resolution record of northern hemisphere climate extending into the last interglacial period. Nature 431, 147–151.
Paulsen, D.E., Li, H.C., Ku, T.L., 2003. Climate variability in central China over the last 1270 years revealed by high-resolution stalagmite records. Quaternary Science Review 22, 691–701.
Petit, J.R., Jouzel, J., Raynaud, D., Barkov, N.I., Barnola, J.-M., Basile, I., Bender, M., Chappellaz, J., Davis, M., Delaygue, G., Delmotte, M., Kotlyakov, V.M., Legrand, M., Lipenkov, V.Y., Lorius, C., Pepin, L., Ritz, C., Saltzman, E., Stievenard, M., 1999. Climate and atmospheric history of the past 420,000 years from the Vostok ice core, Antarctica. Nature 399, 429–436.
Prell, W.L., Kutzbach, J.E., 1987. Monsoon variability over the past 150,000 years. Journal of Geophysical Research 92, 8411–8425.
Prell, W.L., Kutzbach, J.E., 1992. Sensitivity of the Indian monsoon to forcing parameters and implications for its evolution. Nature 360, 647–652.
Shakun, J.D., Burns, S.J., Fleitmann, D., Kramers, J., Matter, A., Al-Subary, A., 2007. A high-resolution, absolute-dated deglacial speleothem record of Indian Ocean climate from Socotra Island, Yemen. Earth and Planetary Science Letters 259, 442–456.
Shen, C.C., Edwards, R.L., Cheng, H., Dorale, J.A., Thomas, R.B., Moran, S.B., Weinstein, S.E., Edmonds, H.N., 2002. Uranium and thorium isotopic and concentration measurements by magnetic sector inductively coupled plasma mass spectrometry. Chemical Geology 185, 165–178.
Shen, C.-C., Cheng, H., Edwards, R.L., Moran, S.B., Edmonds, H.N., Hoff, J.A., Thomas, R.B., 2003. Measurement of attogram quantities of ^{231}Pa in dissolved and particulate fractions of seawater by isotope dilution thermal ionization mass spectroscopy. Analytical Chemistry 75, 1075–1079.
Shen, C.-C., Li, K.-S., Sieh, K., Natawidjaja, D., Cheng, H., Wang, X., Edwards, R.L., Lam, D.D., Hsieh, Y.-T., Fan, T.-Y., Meltzner, A.J., Taylor, F.W., Quinn, T.M., Chiang, H.-W., Kilbourne, K.H., 2008. Variation of initial $^{230}Th/^{232}Th$ and limits of high precision U–Th dating of shallow-water corals. Geochimica et Cosmochimica Acta 72, 4201–4223.
Solanki, S.K., 2002. Solar variability and climate change: is there a link? Adytonomy & Geophysics 43, 5.09–5.13.
Soon, W., Posmentier, E., Baliunas, S., 2000. Climate hypersensitivity to solar forcing? Annales Geophysicae 18, 583–588.

Tao, S.Y., Chen, L.X., 1988. A Review of Recent Research on the East Asian Summer Monsoon in China. In: Tao, S.Y. (Ed.), Monsoon Meteorology. Oxford University Press, Oxford, pp. 60–92.

Thompson, L.G., Yao, T.D., Davis, M.E., Henderson, K.A., Thompson, E.M., Lin, P.N., Beer, J., Synal, H.A., Dai, J.C., Bolzan, J.F., 1997. Tropical climate instability: the Last Glacial cycle from a Qinghai – Tibetan ice core. Science 276, 1821–1825.

Waelbroeck, C., Frank, N., Jouzel, J., Parrenin, F., Masson-Delmotte, V., Genty, D., 2008. Transferring radiometric dating of the last interglacial sea level high stand to marine and ice core records. Earth and Planetary Science Letters 265, 183–194.

Wang, Y.J., Cheng, H., Edwards, R.L., An, Z.S., Wu, J.Y., Shen, C.-C., Dorale, J.A., 2001. A high-resolution absolute-dated late Pleistocene monsoon record from Hulu Cave, China. Science 294, 2345–2348.

Wang, Y.J., Cheng, H., Edwards, R.L., He, Y., Kong, X., An, Z., Wu, J., Kelly, M.J., Dykoski, C.A., Li, X., 2005. The Holocene Asian monsoon: links to solar changes and north Atlantic climate. Science 308, 854–857.

Wang, X., Auler, A.S., Edwards, R.L., Cheng, H., Ito, E., Solheid, M., 2006. Interhemispheric anti-phasing of rainfall during the last glacial period. Quaternary Science Reviews 25, 3391–3403.

Wang, Y.J., Cheng, H., Edwards, R.L., Kong, X., Shao, X., Chen, S., Wu, J., Jiang, X., Wang, X., An, Z., 2008. Millennial- and orbital-scale changes in the East Asian monsoon over the past 224,000 years. Nature 451, 1090–1093.

Wang, B., 2007. The Asian Monsoon. Springer Praxis Publishing, Chichester, UK, ISBN 3-540-40610-7, 787 p.

Wei, K.-Y., Chiu, T.-C., Chen, Y.-G., 2003. Toward establishing a maritime proxy record of the East Asian summer monsoons for the late Quaternary. Marine Geology 201, 67–79.

Winogard, I.J., Coplen, T.B., Landwehr, J.M., Riggs, A.C., Ludwig, K.R., Szabo, B.J., Kolesar, P.T., Revesz, K.M., 1992. Continuous 500,000-year climate record from vein calcite in Devils Hole, Nevada. Science 258, 255–260.

Winogard, I.J., Landwehr, J.M., Ludwig, A.C., Coplen, T.B., Riggs, A.C., 1997. Duration and structure of the pas four interglaciations. Quaternary Research 48, 141–154.

Winogard, I.J., Landwehr, J.M., Coplen, T.B., Sharp, W.D., Riggs, A.C., Ludwig, K.R., Kolesar, P.T., 2006. Devils Hole, Nevada, $\delta^{18}O$ record extended to the mid-Holocene. Quaternary Research 66, 202–212.

Winogard, I.J., 2002. The California current, Devils Hole, and Pleistocene climate. Science 296, 7.

Yuan, D., Cheng, H., Edwards, R.L., Dykoski, C.A., Kelly, M.J., Zhang, M., Qing, J., Lin, Y., Wang, Y., Wu, J., Dorale, J.A., An, Z., Cai, Y., 2004. Timing, duration, and transition of the last interglacial Asian monsoon. Science 304, 575–578.

Zhang, J.C., Liu, Z.G., 1992. Climate of China. Wiley, New York. p. 376.

Zhang, P., Cheng, H., Edwards, R.L., Chen, F., Wang, Y., Yang, X., Liu, J., Tan, M., Wang, X., Liu, J., An, C., Dai, Z., Zhou, J., Zhang, D., Jia, J., Jin, L., Johnson, K.R., 2008. A test of climate, sun, and culture relationships from an 1810-year Chinese cave record. Science 322, 940–942.

Zhang, D.E., Li, H.-C., Ku, T.-L., Lu, L.H., 2010. On linking climate to Chinese dynastic change: spatial and temporal variations of monsoonal rain. Chinese Science Bulletin 55, 77–83.

Zhao, Z.C., Wang, S.W., 1979. Interaction between the circulation and climate in Northern and Southern Hemispheres. Acta Meteorologica Sinica 37, 59–68 (in Chinese with English abstract).